ISSN 1063-7710, Acoustical Physics, 2011, Vol. 57, No. 2, pp. 144–150. © Pleiades Publishing, Ltd., 2011.

PHYSICAL ACOUSTICS

Compensation of Fat Layer Effects in Ultrasound Imaging Using an Inclined-Fat-Layer Model Derived from Magnetic Resonance Images[1]

A. B. M. Aowlad Hossain[a], L. H. Kang[a], J. S. Kim[b], M. H. Cho[a], and S. Y. Lee[a]

[a] *Department of Biomedical Engineering, Kyung Hee University, Republic of Korea*
e-mail: sylee01@khu.ac.kr

[b] *R&D Center, GE Ultrasound, Republic of Korea*

Received September 30, 2009

Abstract—When cutaneous fat layers are in the ultrasound imaging region, the phase aberration caused by the fat layers induce image distortion as well as spatial resolution degradation. The phase aberration may complicate clinical procedures particularly when ultrasound imaging is employed for spatial positioning of medical devices like a biopsy needle or HIFU. To compensate the fat layer effects more precisely in beamforming, an inclined-fat-layer model has been established from the magnetic resonance images of the same imaging region as in the ultrasound scanning. We have verified utility of the fat layer model by taking images of a metal needle put into an inclined-fat-layer mimicking phantom. The ultrasound images taken with a 128-element linear phase array operating at 6 MHz have shown better resolution and less distortion when receive beamforming was performed with the phase delay data derived from the inclined-fat-layer model.

DOI: 10.1134/S1063771011020205

INTRODUCTION

Depending on tissue composition and temperature, sound speeds in biological tissues vary from around 1460 m/s for fat to 1600 m/s for muscle, with other tissues like liver, blood, kidney in the range of 1540–1560 m/s [1]. In tissue imaging by an ultrasound scanner, inhomogeneous sound speed distribution in the imaging region causes phase aberration of ultrasound beam which may result in distortion and resolution degradation in ultrasound images [2]. The most severe phase aberration appears when the tissues of interest are located under thick fat layers as often found in clinical imaging.

Many types of multimodal imaging modalities such as PET/CT or PET/MR have been developed to exploit complementary features from two different imaging devices. Combining ultrasound imaging with other imaging modalities like MRI is now much desired in the clinical field particularly for ultrasound-imaging-guided biopsy after locating malignant tissues using MRI [3, 4]. In ultrasound-imaging-guided biopsy with MRI, MRI images are first taken to identify and locate the malignant tissues. After the MRI scan of the subject lying prone on a specially designed couch for both MRI and ultrasound scanning, the subject is transferred to the biopsy room. The MRI images are then co-registered with the ultrasound images to indicate the targeted region during ultrasound-imaging-guided biopsy [3]. To avoid any possible mismatches of the targeted tissues during MRI and ultrasound scanning, the simultaneous MRI and ultrasound imaging method has been recently introduced [4]. It has been reported that ultrasound images can be taken simultaneously with MRI in a time-multiplexed way without any noticeable interference between MRI and ultrasound. It seems that combination of MRI and ultrasound scanning would be further developed in the near future due to their complementary features.

In biopsy, locating the needle precisely at the tissue of interest is crucial. In ablation therapy using high intensity focused ultrasound (HIFU), locating the HIFU beam precisely on the malignant tissue is also crucial not to ablate nearby normal tissues [5–7]. In virtual biopsy in which ultrasound push beam is applied to the tumor region to quantify the tissue stiffness, precisely locating the ultrasound beam on the tumor is also important [8]. Fat layers in the human body may complicate the above mentioned procedures since it often induces so big phase aberration as to compromise the image quality in terms of image resolution and distortion. Fat region in MRI is highly contrasted against non-fatty tissues since fatty tissues have much different MRI parameters, such as spin-spin relaxation time (T_2) or spin-lattice relaxation time (T_1). Therefore, delineation of the fat regions from MR images can be incorporated into ultrasound imaging to compensate the phase aberration effects. In this

[1] The article is published in the original.

paper, we introduce a phase aberration correction method in which the geometric information about the fat layer taken from the magnetic resonance images is exploited in ultrasound beamforming.

There have been many reports on phase aberration correction methods in ultrasound imaging [9–14]. Although phase aberration correction has been already implemented successfully in some commercially available ultrasound imaging systems, little is known about the algorithms that are needed to improve the image quality in terms of image distortion and spatial resolution [12, 13]. Most of the previous phase aberration correction methods use parallel fat layer model. In this study, we use an inclined-fat-layer model to better compensate the phase aberration, and we estimate the thickness and inclination angle of the fat layer from the magnetic resonance images. With the estimated fat layer thickness and inclination angle and with presumed sound velocities in fatty and non-fatty tissues, we try to compensate the phase aberration effects in the beamforming. Experimental results of fat-layer-mimicking phantom imaging with a 6 MHz linear probe are presented along with simulation results.

DERIVATION OF TIME DELAYS FROM THE INCLINED-FAT-LAYER MODEL

To examine effects of a cutaneous fat layer on beamforming quality, we plan a two-layer model which has an inclined interface with a constant slope as shown in Fig. 1. The actual interface should be mostly curved, rather than linear, in most regions of a human body. We presume here that the inclined-two-layer model better approximate the actual interface than the conventional parallel fat layer model. We can also approximate a curved interface by a piecewise linear model in which each piece has an inclined interface.

The interface between the two layers is inclined by the angle of γ. If the layers are parallel, we simply need to set $\gamma = 0$ in the following derivations. The propagation mediums of the top and bottom layers are fatty and non-fatty tissues, respectively. With the model shown in Fig. 1, we are to calculate propagation delay times from each transducer element to a focal point A to derive the time delay data for phase aberration correction in beamforming. The sound speeds of the top and bottom layers are denoted as c_1 and c_2, respectively. On top of the top layer, N transducer elements are uniformly placed with the inter-element spacing of Δ. The propagation delay time can be calculated from the geometrical relationship of an acoustic ray path through the medium of different velocity.

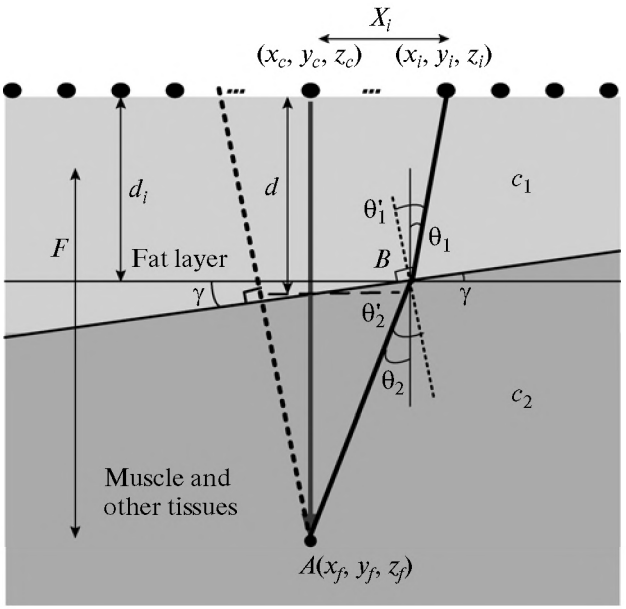

Fig. 1. Derivation of time delays for the inclined-fat-layer model.

The delay time for the ith transducer element at (x_i, y_i, z_i) as compared to center element at (x_c, y_c, z_c) in Fig. 1 is now to be derived. The propagation delay time from the ith element to the focal point A at (x_f, y_f, z_f) is:

$$t_p = \frac{d_i}{c_1 \cos\theta_1} + \frac{F - d_i}{c_2 \cos\theta_2}, \tag{1}$$

where d_i is the perpendicular distance from the top surface to the refraction point B on the interface. F is the focal depth and θ_1 and θ_2 are the angle of incidence of the acoustic ray in the top and bottom layers, respectively. From the geometry:

$$\begin{aligned} |d - d_i| &= (|X_i| - d_i \tan\theta_1)\tan\gamma, \\ d_i \tan\theta_1 + (F - d_i)\tan\theta_2 &= |X_i|, \end{aligned} \tag{2}$$

where d is the perpendicular distance from the center element to the interface, that is, the fat layer thickness at the center, X_i is the distance from the center element to the ith element, and γ is the inclination angle of the interface between the two layers. Snell's law of refraction states:

$$\frac{\sin\theta_1'}{c_1} = \frac{\sin\theta_2'}{c_2}, \tag{3}$$

where the angle of incidence is redefined with respect to the inclined interface. Depending on θ_2, the angles θ_1' and θ_2' can be found as:

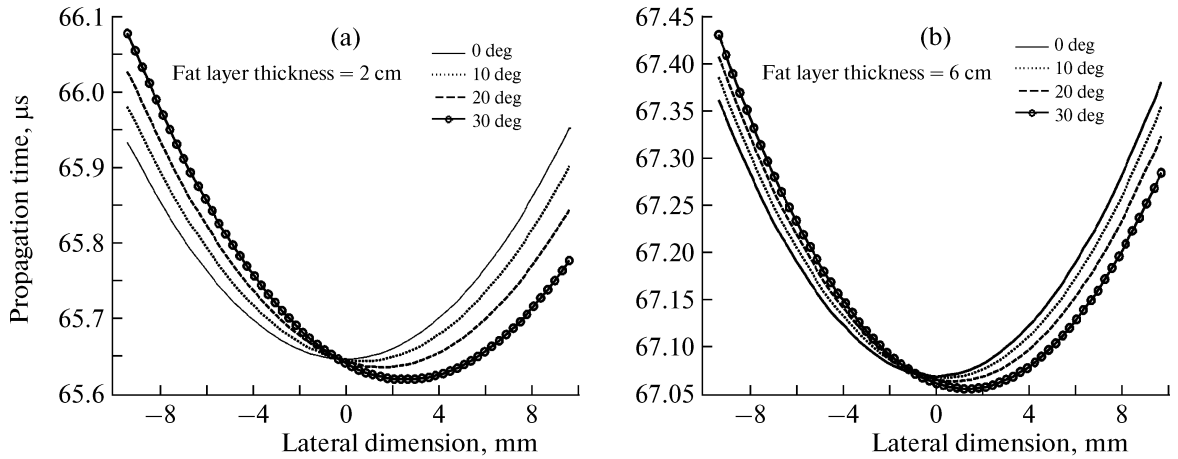

Fig. 2. Propagations times from a focal depth of 10 cm along a 64-element linear probe.

$$\theta_1' = \begin{cases} \theta_1 + \gamma & (\theta_2 \geq 0) \\ \gamma - \theta_1 & (-\gamma \leq \theta_2 < 0) \\ \theta_1 - \gamma & (\theta_2 < -\gamma) \end{cases}$$

$$\theta_2' = \begin{cases} \theta_2 + \gamma & (\theta_2 \geq 0) \\ \gamma - \theta_2 & (-\gamma \leq \theta_2 < 0) \\ \theta_2 - \gamma & (\theta_2 < -\gamma) \end{cases} \quad (4)$$

We use numerical methods to solve the above equations to find the values of θ_1, θ_2 and d_i which are necessary to determine the propagation time t_p. Figure 2 shows the delay times at every element with respect to the center element when a 64-element linear probe with inter-element spacing of 0.3 mm is employed to take images at a focal depth of 10 cm. It shows two different fat thicknesses, 2 cm and 6 cm, with different inclination angles. From Fig. 2, we can notice the delay curves shift from the symmetric one and the amount of shifts increases as the inclination angle increases.

COMPENSATION OF THE INCLINED-FAT-LAYER EFFECTS

With the time delay data derived from the inclined-fat-layer model, we compensate the fat layer effect in the receive beamforming. We first see the effect of the inclined-fat-layer in the receive beamforming by comparing the receive beam profiles obtained with and without the compensations. In the case of no compensations in the receive beamforming, we apply the time delay data derived from the homogeneous medium model with the nominal sound speed of 1540 m/s at transducer elements.

In calculating the receive beam profile, we assume uniform irradiation of transmit ultrasound beam all over the imaging region and also assume uniform echogenic scatterer distribution along the lateral direction. With arranging uniform echo sources along the lateral direction at a given focal depth, we calculate the receive beam profiles by summing up all the echo signals after applying the time delays derived from the incline-fat-layer model or the uniform medium model at each transducer element. Let r_{ij} is the geometrical distance between the jth source and the ith receiving element. In the layered medium, the ultrasound beam refracts at the interface. Let $r_{ij,1}$ and $r_{ij,2}$ be the propagation path lengths in the top and bottom layers, respectively, when sound wave propagates from the jth source to the ith receiving element. Then, the receive beam profile is given as:

$$P(j) = \frac{1}{N}\sum_{i=1}^{N} e^{-2\pi f\left(\frac{r_{ij,1}}{c_1} + \frac{r_{ij,2}}{c_2} - t_i^F\right)}, \quad j = 1, 2, \ldots, M, \quad (5)$$

where t_i^F is the time delay for receive beamforming at a focal depth F. The time delays are derived either from the inclined-fat-layer model for the compensated case or from the uniform medium model for the uncompensated case. In the uniform medium model, uniform distribution of a non-fatty tissue with sound speed of 1540 m/s is assumed.

The calculated received beam profiles at a focal depth of 10 cm are shown in Fig. 3 for several combinations of fat layer thickness and inclination angle. In this calculation, we considered a 64-element linear array with inter-element spacing of 0.3 mm. The sound speeds of the fat layer and non-fatty layer are 1460 m/s and 1540 m/s, respectively. The uncompensated beam profiles are shown by dotted lines while

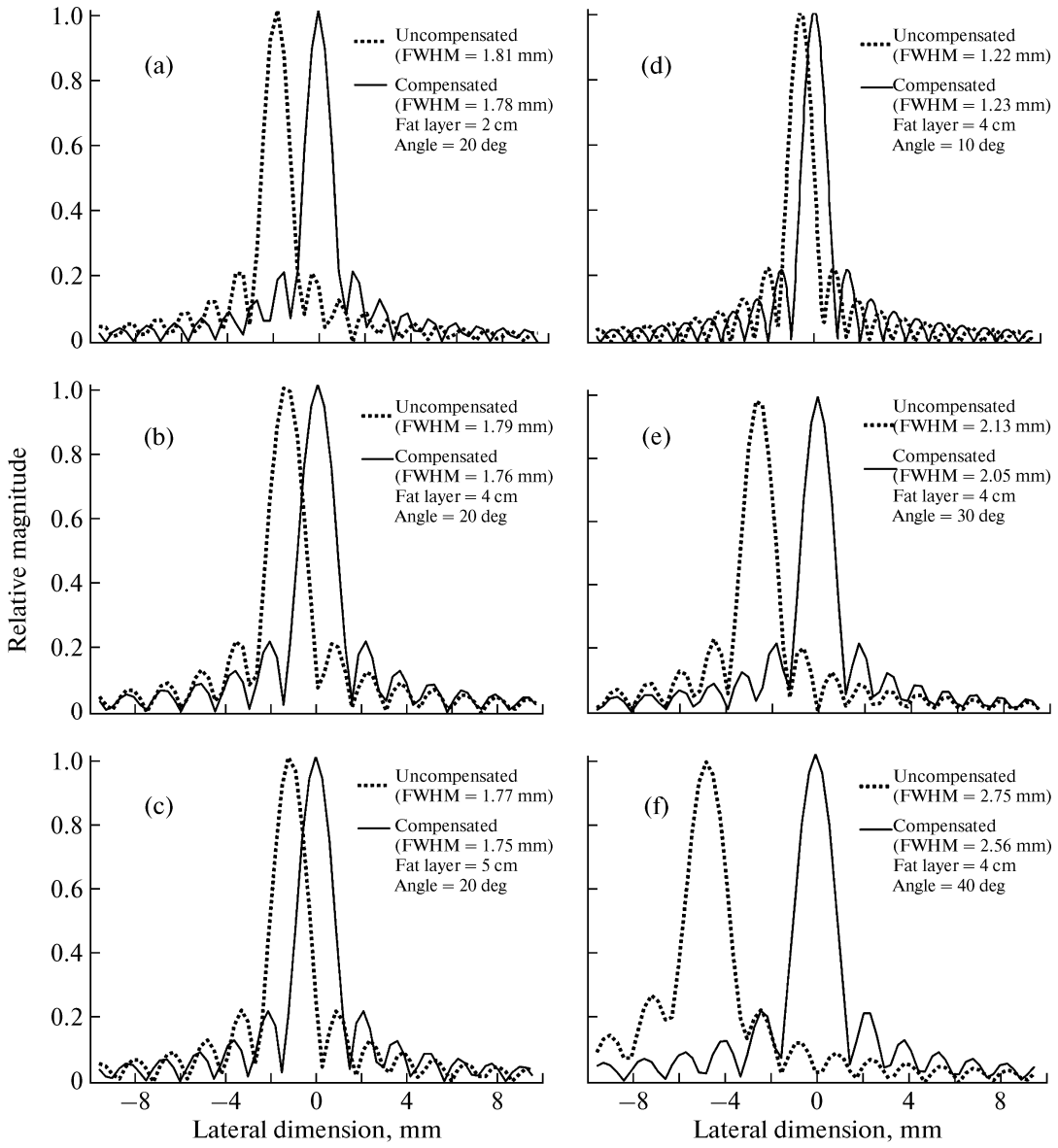

Fig. 3. Received beam profiles at a focal depth of 10 cm for different thickness and inclination angle of the fat layer. Solid and dotted curves in (a) through (f) represent the beam profile obtained with and without phase aberration compensations, respectively.

compensated beam profiles by solid lines. We can notice clear tendency that the amount of beam shift increases as the inclination angle increases. Even though it is not clearly noticeable, the fat layer also widens the beam profiles, which would degrade lateral resolution of ultrasound images. By applying the time delays derived from the inclined-fat-layer model, the beam shift as well as the beam widening is corrected. In terms of the full-width-half-maximum (FWHM) at the main lobe of the receive beam profiles, the FWHMs of the received beam profiles are reduced by 1.7–7.5% after the compensation. The beam shifts in the lateral direction are an order of mm, which would be noticeable in the ultrasound images.

The pixel shifts caused by the fat layer can be corrected by applying the time delay data derived from the inclined-fat-layer model. Figure 4 shows a simulated situation of a thin biopsy needle put into an inclined-fat-layer model. The top layer thickness is 30 mm at the center and the inclination angle is 30 degrees. The sound speeds of the fat layer and non-fatty layer are again 1460 m/s and 1540 m/s, respectively. The needle insertion angle is 60 degrees with respect to the horizontal axis. If we have receive beamforming without compensating the fat layer effect, it is inevitable to have pixel shifts. To estimate the needle shape in the ultrasound images without the compensation, we have calculated the amount of lateral shift on the needle

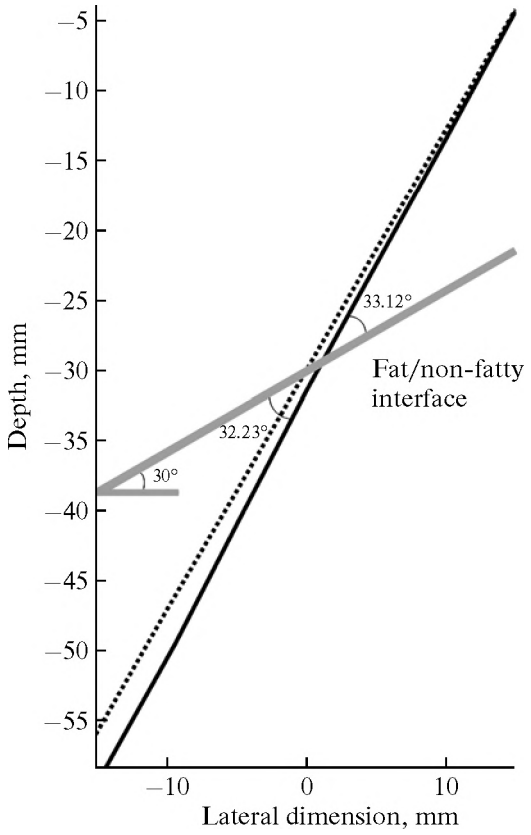

Fig. 4. Simulated needle position (solid line) when the fat layer effects are uncompensated. The original needle position is shown using the dashed line.

Fig. 5. A magnetic resonance image of the inclined-fat-layer phantom.

position at every depth. As can be noticed from Fig. 3, the fat layer thickness and the inclination angle determine the amount of lateral shift at a given depth. By tracking the amount of lateral shifts at every depth on the needle position, we estimated the needle image in uncompensated ultrasound images. The distorted needle position is shown by the solid line in Fig. 4 along with the original needle position by the dashed line. Due to the fat layer effects, the needle looks more inclined, 33.12 degrees in the top (fat) layer and 32.23 degrees in the bottom (non-fatty) layer from the interface, than it does in its original position.

EXPERIMENTAL RESULTS

We have made a phantom using polysaccharide (agar), n-propanol, and distilled water to implement the inclined-fat-layer model. We have chosen agar as tissue equivalent material because its sound speed is similar to those of tissues ranging from 1500 m/s to 1600 m/s at room temperature. Sound speed of agar-water–propanol mixture varies in linear fashion with the concentration of *n*-propanol at constant temperature [15]. The upper layer has a thickness of 4 cm at the center and was made of only agar and water to mimic a fat layer. The 10 cm thick lower layer was made of agar, water and 25% n-propanol to mimic a non-fatty layer. The agar phantom has the size of 20 cm × 20 cm × 15 cm. To calculate the time delays based on the exact sound speed of each layer, we measured the sound speeds in the layers by separate A-mode experiments. It has been found that the upper and lower layers have the sound speeds of 1505 m/s and 1610 m/s, respectively.

Before ultrasound imaging, we took magnetic resonance images of the phantom using a 3.0 Tesla whole body MRI system (Medinus Co., Korea) to measure the actual thickness and the inclination angle. The MRI scan parameters, TR and TE, were 550 and 13 ms, respectively, in a spin echo imaging sequence. One of the magnetic resonance images is shown in Fig. 5 from which the inclination angle was found to be 27 degrees. For ultrasound imaging, we used a commercial ultrasound scanner GE LOGIQ P5 operating at 6 MHz with a linear probe. The linear probe has 128-elements with the element-to-element spacing of 0.3 mm. The demodulated I/Q data were acquired with the sampling time of 0.3 μs in a complex data format. After acquiring the IQ data, we performed receive beamforming offline using the time delay data derived from the inclined-fat-layer model.

The linear probe was placed at the center of the phantom. We inserted a metallic acupuncture needle, 9 cm long and 0.5 mm wide, into the phantom with an insertion angle of 62 degrees to mimic biopsy operation. Figure 6 shows the needle images obtained with or without the fat layer effect compensation. Without compensation, the needle image is severely blurred and a little deflected on the interface. But, the blurring effect is greatly reduced after the compensation. Figure 7 compares cut views over the needle region in the bottom layer. To show the distortion correction, we

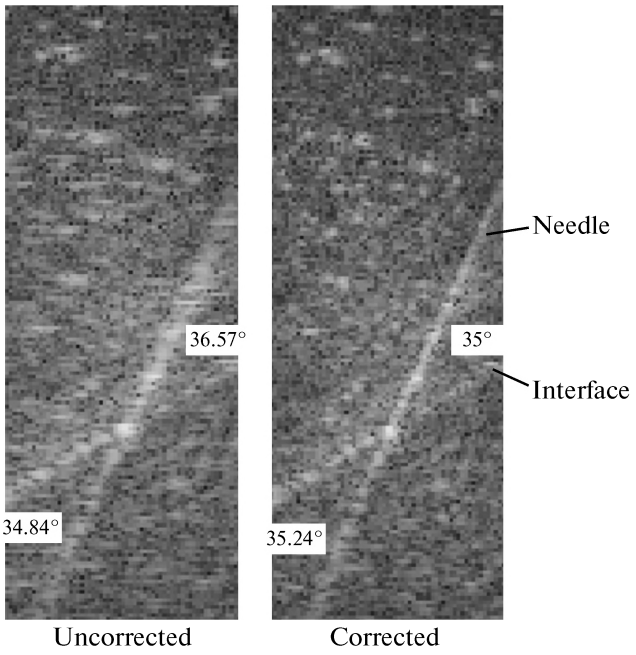

Fig. 6. Needle images obtained with or without the fat layer effect compensation.

measured vertical angles between the layer interface and the needle. In the uncompensated image, the vertical angles are different by 1.73 degrees due to the image distortion. But, the difference is reduced to 0.24 degrees in the compensated image.

DISCUSSIONS AND CONCLUSIONS

Fat layers often degrade image quality in ultrasound imaging to the extent that clinical utility of ultrasound images is compromised. If the shape of the fat layer is known prior to ultrasound scanning, the shape information can be incorporated into ultrasound beamforming to better compensate the fat layer effects. In this study, we have shown that the ultrasound image quality in terms of distortion and resolution can be improved with aids of MRI. Since MRI can provide spatial information about the fat layers without any spatial distortion, the spatial information can be used for compensating the fat layer effect in the ultrasound beamforming. To use the proposed method practically, however, we need further developments. Firstly, we need automatic and fast co-registration between MRI and ultrasound images. Since ultrasound images mostly have smaller field-of-view than MRI, it is known that co-registration of ultrasound images with images taken with other imaging modalities is technically challenging. Furthermore, deformation of the tissues caused by pressing the transducer on them during the ultrasound scanning complicates the co-registration. Ultrasound scanning inside an MRI magnet is another issue. Even though some researchers have reported a fully integrated MRI-ultrasound imaging system in which MRI and ultrasound scans are performed in a time-multiplexed way to get MRI and ultrasound images simultaneously, it seems that manipulating a ultrasonic transducer inside an MRI magnet still needs many technical developments.

In conclusion, the fat layer effects on ultrasound imaging can be compensated by applying the time delay data derived from magnetic resonance images to beamforming. We expect the proposed method can be used to improve accuracy of needle positioning in ultrasound-imaging-guided biopsy based on multimodal imaging platform of MRI and ultrasound.

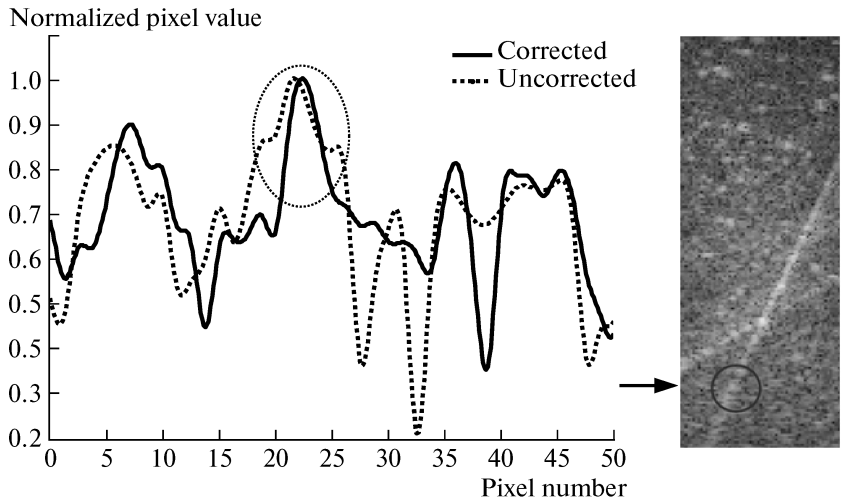

Fig. 7. Cut views of the needle image in the bottom layer. The circled region in the cut views indicates the needle region.

ACKNOWLEDGMENTS

This study was supported by the grants from the National Research Foundation of Korea (2009-0078310) and the grant from the Ministry of Knowledge and Economy of Korea (10033627).

REFERENCES

1. C. R. Hill, J. C. Bamber, and G. R. ter Haar, *Physical Principles of Medical Ultrasonics* (Wiley, 2004).
2. Q. Chen and J. Zagzebski, Ultrasound Med. Biol. **30**, 1297 (2004).
3. C. A. Piron, P. Causer, R. Jong, R. Shumak, and D. B. Plewes, IEEE Trans. Med. Imag. **22**, 1100 (2003).
4. L. Curiel, R. Chopra, and K. Hynynen, IEEE Trans. Med. Imag. **26**, 1740 (2007).
5. G. ter Haar and C. Coussios, Int J. Hyperthermia **23**, 89 (2007).
6. M. R. Bailey, V. A. Khokhlova, O. A. Sapozhnikov, S. G. Kargl, and L. A. Crum, Akust. Zh. **49**, 437 (2003) [Acoust. Phys. **49**, 369 (2003)].
7. V. I. Goland and L. M. Kushkuley, Akust. Zh. **55**, 481 (2009) [Acoust. Phys. **55**, 496 (2009)].
8. S. Chen, M. W. Urban, C. Pislaru, R. Kinnick, Y. Zheng, A. Yao, and J. F. Greenleaf, IEEE Trans. UFFC **56**, 55 (2009).
9. B. A. Abrahim, Z. A. Mustafa, and Y. M. Kadah, Proc. ICCES (2007).
10. S. W. Flax and M. O'Donnel, IEEE Trans. UFFC **35**, 768 (1988).
11. G. C. Ng, S. S. Worrell, P. D. Freiburger, and G. E. Trahey, IEEE Trans. UFFC **41**, 631 (1994).
12. K. W. Rigby, C. L. Chalek, B. H. Haider, R. S. Lewandowski, M. O'Donnell, L. S. Smith, and D. G. Wildes, Proc. IEEE Ultrason. Symp. **2**, 1645 (2000).
13. K. W. Rigby, Proc. SPIE Med. Imag. **3982**, 342 (2000).
14. M. H. Cho, L. H. Kang, J. S. Kim, and S. Y. Lee, Ultrasonics **49**, 774 (2009).
15. M. M. Burlew, E. L. Madsen, J. A. Zagzebski, R. A. Banjavic, and S. W. Sum, Radiology **134**, 517 (1980).